On the origin of the electron blocking effect by an n-type AlGaN electron blocking layer

Zi-Hui Zhang, Yun Ji, Wei Liu, Swee Tiam Tan, Zabu Kyaw, Zhengang Ju, Xueliang Zhang, Namig Hasanov, Shunpeng Lu, Yiping Zhang, Binbin Zhu, Xiao Wei Sun, and Hilmi Volkan Demir

On the origin of the electron blocking effect by an *n*-type AlGaN electron blocking layer

Zi-Hui Zhang,[1,a)] Yun Ji,[1,a)] Wei Liu,[1] Swee Tiam Tan,[1] Zabu Kyaw,[1] Zhengang Ju,[1] Xueliang Zhang,[1] Namig Hasanov,[1] Shunpeng Lu,[1] Yiping Zhang,[1] Binbin Zhu,[1] Xiao Wei Sun,[1,b)] and Hilmi Volkan Demir[1,2,b)]

[1]*LUMINOUS! Centre of Excellence for Semiconductor Lighting and Displays, School of Electrical and Electronic Engineering, School of Physical and Mathematical Sciences, Nanyang Technological University, 50 Nanyang Avenue, Singapore 639798*
[2]*Department of Electrical and Electronics, Department of Physics, and UNAM-Institute of Material Science and Nanotechnology, Bilkent University, TR-06800, Ankara, Turkey*

In this work, the origin of electron blocking effect of *n*-type $Al_{0.25}Ga_{0.75}N$ electron blocking layer (EBL) for $c+$ InGaN/GaN light-emitting diodes has been investigated through dual-wavelength emission method. It is found that the strong polarization induced electric field within the *n*-EBL reduces the thermal velocity and correspondingly the mean free path of the hot electrons. As a result, the electron capture efficiency of the multiple quantum wells is enhanced, which significantly reduces the electron overflow from the active region and increases the radiative recombination rate with holes. © 2014 AIP Publishing LLC. [http://dx.doi.org/10.1063/1.4866041]

InGaN/GaN multiple quantum well (MQW) light-emitting diodes (LEDs) have made significant progress in the past three decades.[1–3] The device performance is, however, still limited by Auger recombination,[4,5] charge separation,[6–9] current crowding,[10–12] insufficient hole injection,[9,13–18] and electron overflow from the MQW active region.[19–22] In order to address these issues, a staggered quantum well architecture and also InGaN/GaN MQWs with Si-step-doped quantum barriers have been proposed to screen the quantum confined Stark effect (QCSE) and increase the spatial overlap of electron-hole wave functions,[7–9] while an improved current spreading can be obtained either by making the *p*-type layer more resistive or the *p*-contact layer more conductive.[10,11] Additionally, an improved crystal quality is also essential for improving the device efficiency.[23] Furthermore, it has been reported that an enhanced hole injection efficiency can be obtained through utilizing a thinner quantum barrier[17,18] or a thinner quantum well.[16] Alternatively, InGaN quantum barriers can also promote the hole injection.[13] Recently, it has been found that *p*-doped quantum barriers favor the hole transport across the InGaN/GaN MQW region.[9,14,15] In addition, substantial efforts have also been devoted to reducing the electron leakage from the InGaN/GaN MQW region. Polarization matched *p*-type electron blocking layer (EBL) and quantum barrier cap layers with a large energy bandgap have been proposed.[19–21] However, the *p*-type electron blocking layer can on one hand reduce the electron overflow, and on the other hand, it also retards the hole injection.[24] Recently, the *n*-type electron blocking layer has also been demonstrated.[25,26] Although the simulations in Refs. 25 and 26 show the advantage of the *n*-EBL over the *p*-type EBL, the physical mechanism of electron blocking effect by the *n*-type EBL has never been clearly elucidated. Thus, in this study, based on powerful numerical simulations, we experimentally investigated effect of the *n*-type EBL by dual-wavelength emission method. Here, we have discovered that the polarization-induced electric field in the *n*-EBL decelerates the thermal velocity of the hot electrons, leading to the electron mean free path reduction, which increases the quantum well capture efficiency for electrons and accounts for the reduced electron leakage from the InGaN/GaN MQW region.

In this work, two InGaN/GaN LED samples as shown schematically in Figs. 1(a) and 1(b) with dual emission wavelengths have been designed and grown by a metal-organic chemical vapor deposition (MOCVD) system. The epitaxial growth was initiated from a $c+$ plane sapphire substrate. A 30 nm low-temperature GaN nucleation layer was deposited and followed by a 4 μm high-temperature unintentionally doped GaN (*u*-GaN) template. Then, a 2 μm *n*-GaN layer with an electron concentration of $5 \times 10^{18}\,cm^{-3}$ was grown. For the Reference sample, the MQW regions were grown subsequently. Nevertheless, for the Sample with *n*-EBL, a 25 nm *n*-$Al_{0.25}Ga_{0.75}N$ EBL was grown before the MQW regions and the electron concentration was estimated to be $5 \times 10^{18}\,cm^{-3}$. The MQW regions include two sets of MQW stacks for both the Reference and the Sample with *n*-EBL with five $In_{0.18}Ga_{0.82}N$/GaN quantum wells as the first stack and three $In_{0.10}Ga_{0.90}N$/GaN quantum wells as the second stack. The InN fraction in the quantum wells was controlled by adjusting the growth temperature of 742 and 758 °C for $In_{0.18}Ga_{0.82}N$/GaN and $In_{0.10}Ga_{0.90}N$/GaN MQWs, respectively. Moreover, in order to promote the hole transport across the active region, the quantum barrier thicknesses for both samples have been graded into 12, 11, 10, 9, 8, 7, and 6 nm in the growth direction. The last quantum barrier is kept to be 12 nm to suppress the Mg diffusion.[27] Meanwhile, the quantum well thickness is 3 nm for all wells. Finally, a 0.2 μm *p*-GaN layer was grown, and the effective hole concentration is estimated to be $3 \times 10^{17}\,cm^{-3}$.

a)Z.-H. Zhang and Y. Ji contributed equally to this work.
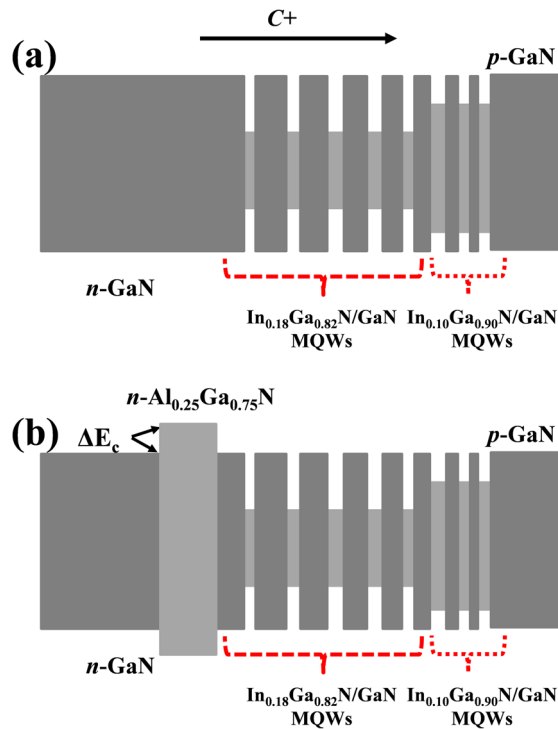b)Electronic addresses: exwsun@ntu.edu.sg and volkan@stanfordalumni.org

(a)

FIG. 1. Schematic energy band diagrams for (a) the Reference sample, and (b) the Sample with *n*-EBL.

Photoluminescence (PL) measurement was conducted on the two samples using a PL mapper system (Nanometric RPM2000). The excitation wavelength of the 15 mW He-Cd laser source is 325 nm. The PL spectra for the Reference and the Sample with *n*-EBL are shown in Fig. 2. It can be seen that both the samples exhibit two emission peaks at around 427 and 467 nm, respectively. The emission spectrum with the shorter peak emission wavelength corresponds to $In_{0.10}Ga_{0.90}N$/GaN MQWs, while the longer one corresponds to $In_{0.18}Ga_{0.82}N$/GaN MQWs. Since there are five pairs of $In_{0.18}Ga_{0.82}N$/GaN MQWs and three pairs of $In_{0.10}Ga_{0.90}N$/GaN MQWs, the PL signal at the longer emission wavelength is stronger than that at the shorter emission wavelength. In addition, the PL intensity for the Sample with *n*-EBL is weaker than that for the Reference, and this can be attributed to the increased QCSE within the MQWs caused by the underneath *n*-EBL.

The electroluminescence (EL) spectra and the optical output power for both the samples have been collected through an integrating sphere attached to an Ocean Optics spectrometer (QE65000). The metal contacts were made by indium balls on the LED dies with a diameter of 1.0 mm. The EL spectra under different injection current levels for both the samples are presented in Figs. 3(a)–3(g). In addition, we also show the ratio of the external quantum efficiency (EQE) for $In_{0.10}Ga_{0.90}N$/GaN MQWs and $In_{0.18}Ga_{0.82}N$/GaN MQWs in Fig. 3(h). Two distinguished wavelength emission regimes have been observed at 5 A/cm^2 in Fig. 3(a) for both of the samples. As the injection current is increased, the emission intensity of the short wavelength regime for the Sample with *n*-EBL is reduced relative to that for the Reference sample, while the emission intensity of the longer wavelength regime for the Sample

with *n*-EBL becomes higher than that for the Reference [see Figs. 3(b)–3(f)]. When the current level exceeds above 35 A/cm^2, the two distinct emission regimes for the Reference can still be observed, while the short emission wavelength regime for the Sample with *n*-EBL is immersed by the long wavelength emission regime according to Fig. 3(g). Here, we found out that the EQE ratio (Fig. 3(h)) for $In_{0.10}Ga_{0.90}N$/GaN MQWs and $In_{0.18}Ga_{0.82}N$/GaN MQWs for the Sample with *n*-EBL is always smaller than that for the Reference within the measured current range. Since both the samples have identical MQW architectures and *p*-GaN layers, the different evolutionary behavior of EL spectra under various injection current levels should not be caused by the holes. Therefore, we attribute this observation to the electron profiles that are different within the MQW regions between the Reference and the Sample with *n*-EBL. This difference in the electron profiles is caused by the insertion of the *n*-EBL, which will be proved theoretically in the following discussion. The integrated optical output power for the Reference and the Sample with *n*-EBL has been shown in Fig. 4. The Sample with *n*-EBL has exhibited a substantial enhancement in the optical power compared to the Reference. The reduced electron leakage for the Sample with *n*-EBL is the main reason for its power enhancement, as will be shown in the discussion next.

In order to reveal the underlying physical mechanism of the *n*-EBL, we have studied the two samples numerically by APSYS.[8] The simulation parameters regarding the Auger recombination coefficient, the Shockley-Read-Hall recombination lifetime and other nitrogen-contained simulation parameters can be found elsewhere, and specifically, considering the dislocation generation due to strain relaxation during the epitaxial growth, we have assumed a 40% polarization level.[8,10,11]

The relationship among the captured electrons by quantum wells, mean free path and injected electrons can be expressed in Eqs. (1) and (2) (Ref. 28)

$$N_{capture} = N_0 \times \left[1 - \exp(-t_{QW}/l_{MFP}) \right], \quad (1)$$
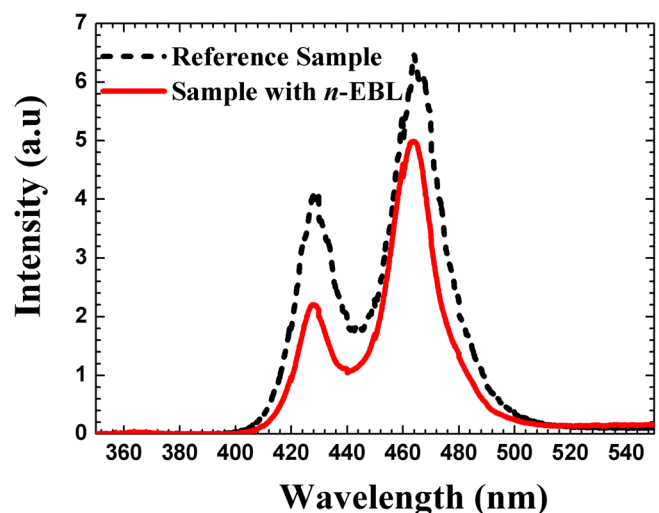
$$l_{MFP} = v_{th} \times \tau_{SC}, \quad (2)$$

FIG. 2. PL spectra for the Reference and the Sample with *n*-EBL.

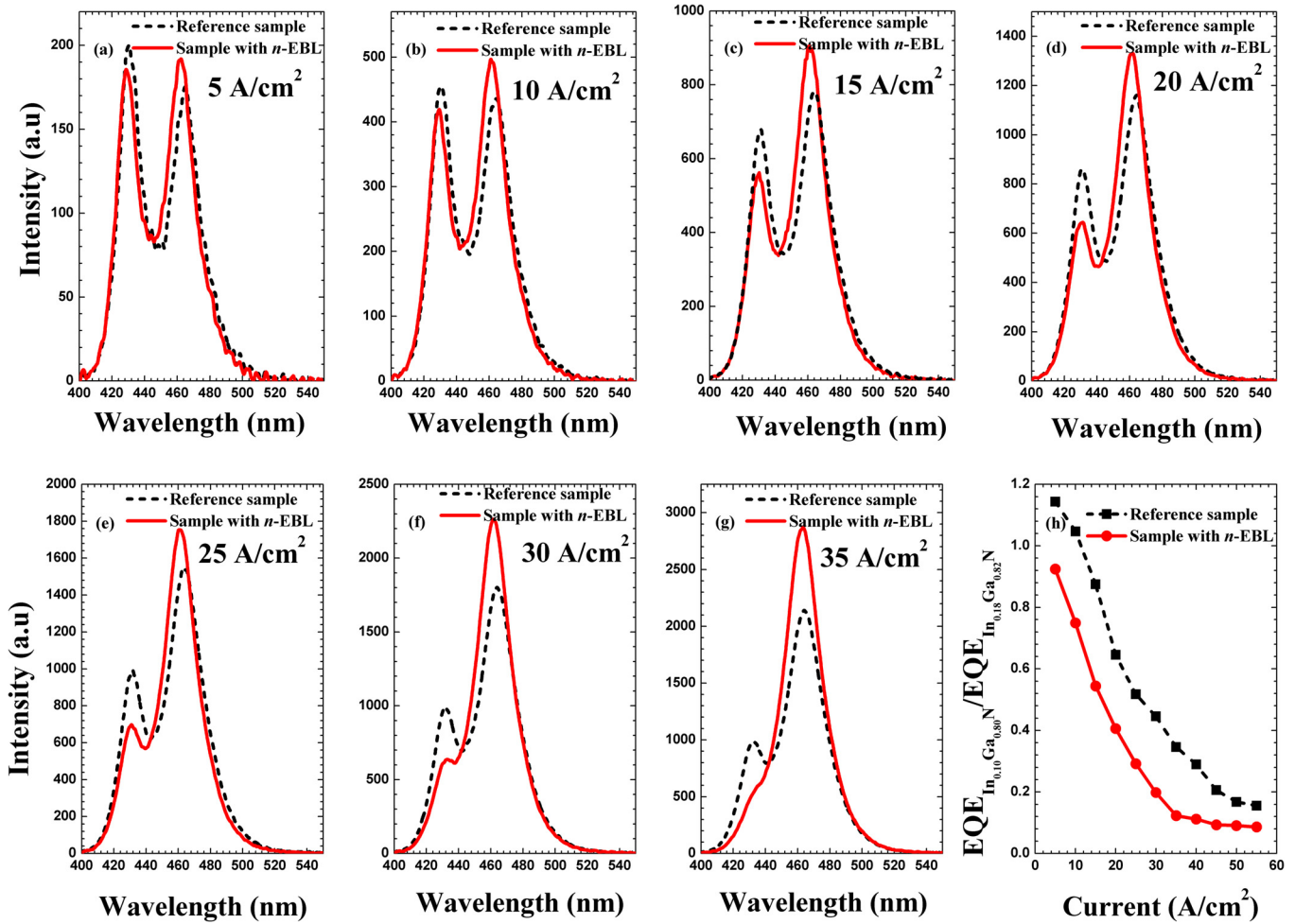FIG. 3. EL spectra for the Reference and the Sample with n-EBL at the current density of (a) 5 A/cm^2, (b) 10 A/cm^2, (c) 15 A/cm^2, (d) 20 A/cm^2, (e) 25 A/cm^2, (f) 30 A/cm^2, (g) 35 A/cm^2, and (h) the ratio of the EQE for In$_{0.10}$Ga$_{0.90}$N/GaN MQWs and In$_{0.18}$Ga$_{0.82}$N/GaN MQWs as a function of the current injection.

where t_{QW} is the quantum well thickness, l_{MFP} is the electron mean free path, and N_0 is the injected electrons, while $N_{capture}$ is the electrons captured by quantum wells. v_{th} is the electron thermal velocity, and τ_{SC} is the scattering time. The schematic model of the electron transport for the InGaN/GaN LED with the n-EBL is depicted in Fig. 5. As illustrated in Fig. 5, Process ① denotes the electrons crossing

the n-EBL and entering the quantum wells for recombination, while Process ② presents the electrons bounced back to the n-GaN layer by the conduction band offset between the n-GaN and the n-EBL layers, leading to a reduction of N_0 in
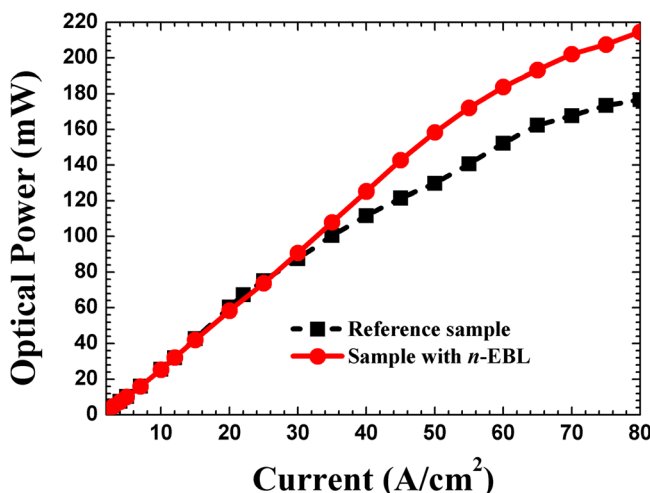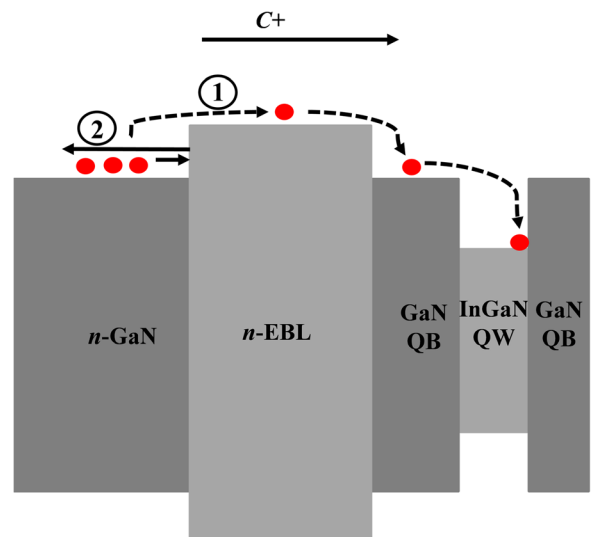

FIG. 5. Schematic electron transport processes for the InGaN/GaN LED with the n-EBL. Here, the electron transport process ① illustrates electrons crossing over the n-EBL and ② shows those being bounced back by the n-EBL. The tunneling process is not considered for simplicity.

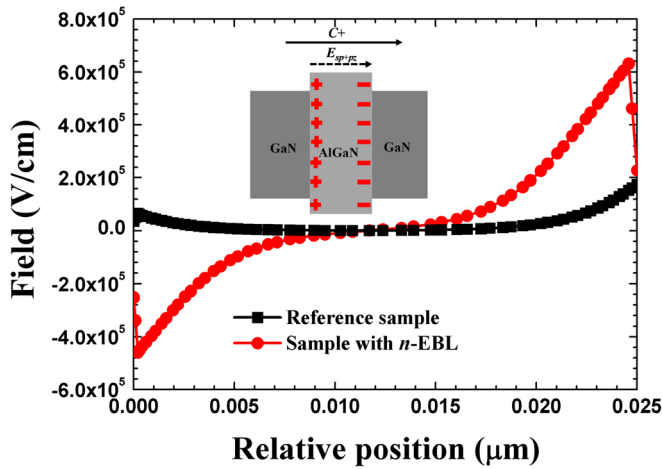FIG. 4. Integrated optical output power of the Reference and the Sample with n-EBL.

FIG. 6. Electric field profiles in the region of the n-EBL layer for the Sample with n-EBL and the GaN layer for the Reference. Inset shows the polarized GaN/AlGaN/GaN heterostructure. The positive direction of the electric field is along the growth orientation, i.e., c+ orientation. The data are collected at the current level of 25 A/cm^2.

Eq. (1). Here, for simplicity, the tunneling electrons through the n-EBL are neglected. This can be justified with the n-EBL thickness making the electron tunneling negligible in this case. According to Eq. (1), the captured electrons are also a function of l_{MFP}, which will be reduced by the n-EBL

as shown next. Therefore, the captured electrons by the MQWs are determined by the competition between the reduction of N_0 due to the potential barrier of the n-EBL and the increase of the capture efficiency due to the reduction in l_{MFP}. The latter will be proved to be dominant, leading to the increased electron capture as follows.

As is well-known, III-nitride epitaxial films grown along c+ orientation exhibit very strong polarization induced electric fields.[6–8,11] Moreover, for GaN/AlGaN/GaN heterostructure [refer to the inset of Fig. 6], the AlGaN layer is subject to the tensile strain, and thus, the piezoelectric field polarization and the spontaneous polarization are both oriented opposite to the growth orientation. Correspondingly, the polarization induced electric field is along the c+ orientation. Since the electric field profile within the n-EBL varies with position, APSYS is used to calculate the resultant electric field (Fig. 6). The electric field within the GaN layer of this region has also been shown for comparison purpose. It is known that the work done by the electric field is given by Eq. (3), which is given by

$$qV = \int_0^t q \times E(y)dy. \tag{3}$$

If qV is positive, then the electrons are decelerated. The integration of the electric field profile in Fig. 6 shows that qV
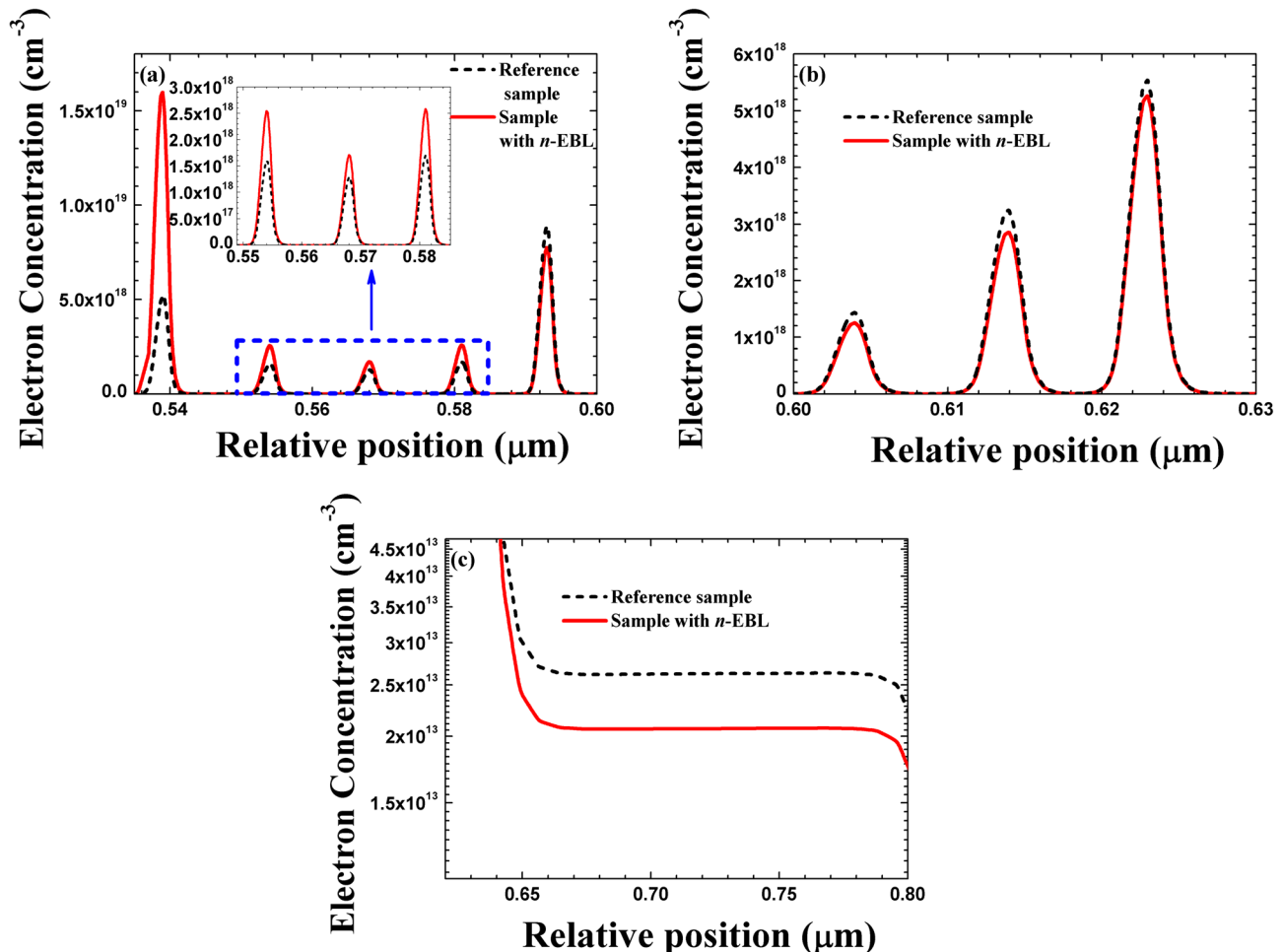
FIG. 7. Electron profiles of the Reference and the Sample with n-EBL (a) for the first five In$_{0.18}$Ga$_{0.72}$N/GaN MQWs in linear scale, (b) for the last three In$_{0.10}$Ga$_{0.90}$N/GaN MQWs in linear scale, and (c) in the p-GaN region in semilog scale. The data are collected at the current level of 25 A/cm^2.

equals 62.6 and 105.7 meV for the Reference and the Sample with n-EBL, respectively. Meanwhile, the thermal velocity can be expressed in Eq. (4) as follows:

$$v_{th} = \sqrt{2 \times [E - qV]/m_e}, \qquad (4)$$

where E is the excess kinetic energy in the n-GaN layer referenced to the conduction band of the n-GaN layer and m_e is the effective mass of electrons. It should be noted that the electrons climb over the n-EBL by gaining potential energy of $\Delta E_{c(GaN/AlGaN)}$ (conduction band offset between the GaN and the n-EBL) while falling down from the n-EBL by losing $\Delta E_{c(GaN/AlGaN)}$, and hence, $\Delta E_{c(GaN/AlGaN)}$ does not appear in Eq. (4). As a result, more negative work is done on electrons, and the thermal velocity of electrons is thus reduced in the device with n-EBL. Based on Eq. (2), l_{MFP} is consequently reduced by the n-EBL, which enables the increase in the electron capture efficiency by MQWs, and hence, the captured electron concentration.

Based on the model, we numerically extracted the electron concentration profiles for the Reference and the Sample with n-EBL, as shown in Figs. 7(a)–7(c). Fig. 7(a) depicts the electron distribution in the first five-pair In$_{0.18}$Ga$_{0.82}$N/GaN MQWs close to the n-GaN layer, and it can be seen that the electron concentration for the LED with n-EBL is higher than that for the Reference sample. The increased electron concentration results from the increased electron capture efficiency by quantum wells after the electron deceleration by the n-EBL. Moreover, the electron profiles in the last three-pair In$_{0.10}$Ga$_{0.90}$N/GaN MQWs neighboring the p-GaN layer in the Reference and the Sample with n-EBL are presented in Fig. 7(b), where the electron concentration of the Sample with n-EBL is found to be reduced compared to that of the Reference. This is reasonable since the deceleration of electrons by the n-EBL causes a reduction in the mean free path, and thus, more electrons are captured by the In$_{0.18}$Ga$_{0.82}$N/GaN MQWs. As a result, the efficiency of electron injection to the In$_{0.10}$Ga$_{0.90}$N/GaN MQWs is lower. The characteristics of the electron distribution in the two MQW stacks explain the behavior of EL spectra evolving under different current levels in Figs. 3(a)–3(h). Furthermore, we demonstrate the electron leakage into the p-GaN layers for both samples in Fig. 7(c). Clearly, it can be seen that the electron leakage for the InGaN/GaN LED with n-EBL is significantly reduced compared to that for the Reference. The reduced electron leakage as a result of the electron blocking effect by the n-EBL accounts for the improved optical output power for the Sample with n-EBL as observed in Fig. 4.

To summarize, the effect of the n-EBL on the electron blocking has been systematically investigated both theoretically and experimentally in this work. Through the analysis of the experimentally observed behavior of the dual-wavelength EL spectra of the Reference and the Sample with n-EBL evolved as a function of current injection levels as well as the theoretical modeling and numerical simulation, the origin of the n-EBL on the reduction of electron overflow has been revealed. The polarization induced electric field caused by the n-EBL decelerates the thermal velocity of electrons and thus the electron mean free path is reduced and the electron capture efficiency by quantum wells is then enhanced.

Consequently, the electron overflow from the active region is suppressed by the n-EBL. Therefore, we conclude that the n-type AlGaN electron blocking layer is very promising for achieving high-performance InGaN/GaN LEDs.

[1]M. H. Crawford, IEEE J. Sel. Top. Quantum Electron. **15**(4), 1028 (2009).
[2]S. T. Tan, X. W. Sun, H. V. Demir, and S. P. DenBaars, IEEE Photon. J. **4**(2), 613 (2012).
[3]N. Tansu, H. P. Zhao, G. Y. Liu, X. H. Li, J. Zhang, H. Tong, and Y. K. Ee, IEEE Photon. J. **2**(2), 241 (2010).
[4]E. Kioupakis, P. Rinke, K. T. Delaney, and C. G. Van de Walle, Appl. Phys. Lett. **98**(16), 161107 (2011).
[5]Y. C. Shen, G. O. Mueller, S. Watanabe, N. F. Gardner, A. Munkholm, and M. R. Krames, Appl. Phys. Lett. **91**(14), 141101 (2007).
[6]J. H. Ryou, P. D. Yoder, J. P. Liu, Z. Lochner, H. Kim, S. Choi, H. J. Kim, and R. D. Dupuis, IEEE J. Sel. Top. Quantum Electron. **15**(4), 1080 (2009).
[7]H. P. Zhao, G. Y. Liu, J. Zhang, J. D. Poplawsky, V. Dierolf, and N. Tansu, Opt. Express **19**(14), A991 (2011).
[8]Z.-H. Zhang, S. T. Tan, Z. G. Ju, W. Liu, Y. Ji, Z. Kyaw, Y. Dikme, X. W. Sun, and H. V. Demir, J. Disp. Technol. **9**(4), 226 (2013).
[9]Z.-H. Zhang, S. T. Tan, Y. Ji, W. Liu, Z. G. Ju, Z. Kyaw, X. W. Sun, and H. V. Demir, Opt. Express **21**(13), 15676 (2013).
[10]Z.-H. Zhang, S. T. Tan, W. Liu, Z. G. Ju, K. Zheng, Z. Kyaw, Y. Ji, N. Hasanov, X. W. Sun, and H. V. Demir, Opt. Express **21**(4), 4958 (2013).
[11]Z.-H. Zhang, S. T. Tan, Z. Kyaw, Y. Ji, W. Liu, Z. G. Ju, N. Hasanov, X. W. Sun, and H. V. Demir, Appl. Phys. Lett. **102**(19), 193508 (2013).
[12]H. Y. Ryu and J. I. Shim, Opt. Express **19**(4), 2886 (2011).
[13]C. H. Wang, S. P. Chang, P. H. Ku, J. C. Li, Y. P. Lan, C. C. Lin, H. C. Yang, H. C. Kuo, T. C. Lu, S. C. Wang, and C. Y. Chang, Appl. Phys. Lett. **99**(17), 171106 (2011).
[14]M. C. Tsai, S. H. Yen, and Y. K. Kuo, IEEE Photonics Technol. Lett. **22**(6), 374 (2010).
[15]Y. Ji, Z.-H. Zhang, S. T. Tan, Z. G. Ju, Z. Kyaw, N. Hasanov, W. Liu, X. W. Sun, and H. V. Demir, Opt. Lett. **38**(2), 202 (2013).
[16]C. H. Wang, S. P. Chang, W. T. Chang, J. C. Li, Y. S. Lu, Z. Y. Li, H. C. Yang, H. C. Kuo, T. C. Lu, and S. C. Wang, Appl. Phys. Lett. **97**(18), 181101 (2010).
[17]M. C. Tsai, S. H. Yen, Y. C. Lu, and Y. K. Kuo, IEEE Photonics Technol. Lett. **23**(2), 76 (2011).
[18]Z. G. Ju, W. Liu, Z.-H. Zhang, S. T. Tan, Y. Ji, Z. B. Kyaw, X. L. Zhang, S. P. Lu, Y. P. Zhang, B. B. Zhu, N. Hasanov, X. W. Sun, and H. V. Demir, Appl. Phys. Lett. **102**(24), 243504 (2013).
[19]M. H. Kim, M. F. Schubert, Q. Dai, J. K. Kim, E. F. Schubert, J. Piprek, and Y. Park, Appl. Phys. Lett. **91**(18), 183507 (2007).
[20]H. P. Zhao, G. Y. Liu, R. A. Arif, and N. Tansu, Solid-State Electron. **54**(10), 1119 (2010).
[21]G. Y. Liu, J. Zhang, C. K. Tan, and N. Tansu, IEEE Photon. J. **5**(2), 2201011 (2013).
[22]X. Ni, X. Li, J. Lee, S. Liu, V. Avrutin, U. Ozgur, H. Morkoc, A. Matulionis, T. Paskova, G. Mulholland, and K. R. Evans, Appl. Phys. Lett. **97**(3), 031110 (2010).
[23]Y. Li, S. You, M. Zhu, L. Zhao, W. Hou, T. Detchprohm, Y. Taniguchi, N. Tamura, S. Tanaka, and C. Wetzel, Appl. Phys. Lett. **98**(15), 151102 (2011).
[24]S. H. Han, D. Y. Lee, S. J. Lee, C. Y. Cho, M. K. Kwon, S. P. Lee, D. Y. Noh, D. J. Kim, Y. C. Kim, and S. J. Park, Appl. Phys. Lett. **94**(23), 231123 (2009).
[25]S. H. Yen, M. C. Tsai, M. L. Tsai, Y. J. Shen, T. C. Hsu, and Y. K. Kuo, IEEE Photonics Technol. Lett. **21**(14), 975 (2009).
[26]Y. Li, Y. Gao, M. He, J. Zhou, Y. Lei, L. Zhang, K. B. Zhu, and Y. L. Chen, J. Disp. Technol. **9**(4), 244 (2013).
[27]H. L. Xing, D. S. Green, H. J. Yu, T. Mates, P. Kozodoy, S. Keller, S. P. Denbaars, and U. K. Mishra, Jpn. J. Appl. Phys., Part 1 **42**(1), 50 (2003).
[28]C. S. Xia, Z. Q. Li, S. Yang, L. W. Cheng, W. D. Hu, and W. Lu, in *Proceedings of the 12th International Conference on Numerical Simulation of Optoelectronic Devices (NUSOD)* (2012), p. 21.